Title

YTHDF3 promotes the progression of gastric cancer by activating Wnt/β-catenin signaling pathway via targeting NEK7

Authors' names

Xiaoran Sun[1,2#] , Shuangshuang Han[1#], Kunyi Liu[1#], Yi Si[1], Mingda Xuan[1], Rui Zhang[1], Jiao Jiao[1], Ting Liu[1], Weifang Yu[1*], Jia Wang[1*]

1 Department of Endoscopy Center, The First Hospital of Hebei Medical University,Shijiazhuang, China

2 Gastroenterology Department, The First Affiliated Hospital of Hebei North University, Zhangjiakou, China

3 Department of Infectious Diseases, The First Hospital of Hebei Medical University, Shijiazhuang, China

# These authors contributed equally

*The corresponding authors.

Corresponding author: Weifang Yu, M.D., Professor, No. 89 Donggang Road,Shijiazhuang, Hebei, China. E-mail: yuweifang@hebmu.edu.cn. Jia Wang, Professor, No. 89 Donggang Road, Shijiazhuang, Hebei, China. E-mail: 57101040@hebmu.edu.cn

Keywords: Gastric cancer; YTHDF3; NEK7; Wnt/β-catenin

Abstract

Gastric cancer is a widespread and deadly malignancy among global digestive tract tumors, alarmingly ranking as the fifth most common cancer in terms of incidence and mortality. Our research, utilizing immunohistochemistry and qRT-PCR, revealed a significant upregulation of YTHDF3 in gastric cancer tissues compared to adjacent non-cancerous tissues. This increased expression of YTHDF3 was found to be closely associated with the incidence of lymph node metastasis and the progression to more advanced TNM stages in patients. *In vitro* experiments demonstrated that YTHDF3 is crucial in promoting the aggressive characteristics of gastric cancer cells by enhancing their ability to proliferate, migrate, and invade, while simultaneously inhibiting apoptosis. The role of YTHDF3 in the progression of gastric cancer was further confirmed by nude mouse subcutaneous tumor model, which showed slowed tumor growth upon YTHDF3 knockdown. This study further confirms through a series of experiments including Co-IP, Co-IF, Western blot, and rescue studies that YTHDF3 promotes the progression of gastric cancer by targeting NEK7 to regulate the Wnt/β-catenin signaling pathway. These pivotal findings highlight the YTHDF3/NEK7/Wnt/β-catenin axis as a promising and accessible therapeutic target for developing new treatments aimed at enhancing the outcomes for gastric cancer patients.

Introduction

Gastric cancer (GC) is one of the most common malignant tumors of the digestive tract worldwide. In 2022, the incidence and mortality rates of gastric cancer ranked

fifth among all cancers globally, accounting for 4.9% of new cancer cases and 6.8% of cancer deaths worldwide[1] . The occurrence and progression of gastric cancer may involve the interaction between oncogenes and tumor suppressor genes, genetics, and environmental factors, and it is a complex multi-step process. Although early-stage gastric cancer patients have a good cure rate and prognosis, advanced gastric cancer often has a poor prognosis and high mortality rate due to the lack of timely and effective treatment methods. With the establishment of public biological databases for gastric cancer and the development of bioinformatics, an increasing number of molecules are considered to be associated with the progression of gastric cancer. Therefore, in-depth study of the molecular mechanisms underlying the development and progression of gastric cancer plays a crucial role in the early diagnosis and precise treatment of gastric cancer.

The YTH domain family proteins (YTHDFs), including YTHDF1, YTHDF2, and YTHDF3, are a class of cytoplasmic m6A-binding proteins defined by the vertebrate YTH domain, which play a broad role in regulating RNA fate. The YTHDF family mediates tumor proliferation, metastasis, and metabolism, and has the potential to serve as predictive and therapeutic biomarkers. The levels of YTH domain proteins are elevated in many malignant tumors[2-4]. Studies indicate that members of the YTH domain protein family, YTHDF1, YTHDF2, and YTHDF3, play pivotal roles in regulating RNA fate and are closely associated with tumor proliferation, metastasis, and metabolism. This phenomenon is observed across various types of cancer, including hepatocellular carcinoma, prostate cancer, pancreatic cancer, gastric cancer, lung cancer, and colorectal cancer [5-10].YTHDF1 primarily promotes translation, YTHDF2 mainly facilitates degradation, and YTHDF3 possesses dual functions of promoting both translation and degradation. This unique positioning suggests that YTHDF3 may act as a bridge or coordinator in the cellular RNA metabolism process.

As a significant member of the YTHDF family, YTHDF3, like other YTHDF

members, contains a C-terminal YTH domain and an N-terminal domain rich in P/Q/N residues. YTHDF3 is located in the cytoplasm. Recent studies have shown that YTHDF3 can directly interact with YTHDF2, affecting mRNA degradation. It can also interact with YTHDF1 to enhance mRNA translation[11], suggesting its potential to modulate diverse signaling pathways and perform multifaceted roles in vivo. Emerging evidence implicates YTHDF3 in the regulation of cancer progression across various types. In triple-negative breast cancer, YTHDF3 stabilizes ZEB1 mRNA, promoting progression and metastasis[12]. Similarly, in ocular melanoma, it enhances cancer stem cell tumorigenicity by promoting CTNNB1 translation[13]and in osteosarcoma, it facilitates aerobic glycolysis through PGK1 stabilization[14]. YTHDF3 can promote the degradation of GAS5 mRNA, thereby enhancing the progression and invasive potential of colorectal cancer[15]. In pancreatic cancer, YTHDF3 engages in a negative feedback loop affecting glycolysis and tumorigenesis[16], while in hepatocellular carcinoma, it promotes progression via the YTHDF3/m6A-EGFR/STAT3 axis and EMT[17]. Additionally, high YTHDF3 expression in colorectal cancer is linked to poor pathological differentiation, advanced stage, and metastasis, driving cancer cell proliferation and migration[18]. These findings underscore the complex and context-dependent roles of YTHDF3 in cancer development, making it a promising target for therapeutic intervention.

However, the exact role of YTHDF3 in the occurrence and progression of GC remains unclear. We found that YTHDF3 is highly expressed in gastric cancer and is closely associated with the poor prognosis of gastric cancer patients. YTHDF3 enhances the malignant phenotype of gastric cancer cells and promotes the growth of gastric cancer in vivo. Through transcriptome sequencing, bioinformatics analysis , Co-IP/Co-IF experiments, and rescue studies, we first discovered that the downstream target gene of YTHDF3 in gastric cancer is NEK7, which is also highly expressed in gastric cancer and interacts with YTHDF3. YTHDF3 upregulates the expression of NEK7 protein and activates the Wnt/β-catenin signaling pathway, further enhancing the proliferation, migration, and invasion abilities of gastric cancer cells, ultimately

promoting the progression of gastric cancer.

Materials and Methods

Patients and samples

We acquired 50 pairs of GC tissues and nearby normal tissues from Hebei Medical University's First Hospital. Before surgery, none of the patients had undergone chemotherapy or radiation, and they had all signed informed permission forms. Following isolation, the aforementioned tissue samples were immediately put in liquid nitrogen before being moved to the First Hospital's Biological Sample Bank at Hebei Medical University for storage. Pathological confirmation of gastric adenocarcinoma/signet-ring cell carcinoma was obtained for the cancer tissues used in this investigation. This study complies with the Declaration of Helsinki's tenets and was authorized by the First Hospital's Ethics Committee at Hebei Medical University (Approval letter No. S00996).

Cell culture

Wuhan Pricella Biotechnology Co., Ltd. provided the human gastric mucosa cell (GES-1) and GC cells (HGC-27, AGS, MKN7, MKN74), which were confirmed by STR analysis. The cells were cultivated in RPMI 1640 medium (Gibco, Gaithersburg, MD, USA) with 1% penicillin-streptomycin solution (Solarbio Sciences & Technology Co. Ltd, Beijing, China) and 10% fetal bovine serum (FBS; Gibco) added as supplements. They were kept in an incubator with 5% carbon dioxide at 37°C and a steady temperature and humidity level. Every month, PCR was used to detect mycoplasma.The cells were utilized for a maximum of 25 passages in each experiment.

Transfections, stable cell lines, siRNAs, shRNAs, and plasmids

Lipofectamine 3000 (Invitrogen, Carlsbad, CA, USA) was used for transfection when the cell confluence in a cell culture flask or dish reached 80–90%. HGC-27 and AGS cells were transfected with YTHDF3 siRNA and a negative control (GenePharma Co., Ltd., Shanghai, China), whereas MKN7 and MKN74 cells were transfected with a YTHDF3 overexpression plasmid and a negative control (GenePharma). HGC-27 cells were also transfected with YTHDF3 shRNA and GenePharma as a negative control. MKN74 cells were transfected with NEK7 siRNA and a GenePharma negative control, while HGC-27 cells were transfected with a NEK7 overexpression plasmid and GenePharma negative control. Experiments were carried out 48 hours following transfection. 48 hours following YTHDF3 shRNA transfection in HGC-27 cells, the cell culture medium was modified to add neomycin at a final concentration of 600 μg/mL (without other antibiotics) in order to establish stable transfected cell lines (HGC-27 shNC, HGC-27 shYTHDF3). Following the formation of the clones, the neomycin concentration was raised to 300 μg/mL and cultured until daybreak.

RNA extraction and qRT-PCR

Using the RNA-Easy Isolation Reagent (Vazyme Biotech Co., Ltd., Nanjing, China), total RNA was extracted from cells and tissues. The PrimeScript RT reagent kit (Takara, Beijing, China) was then used to reverse-transcribe the RNA into complementary DNA (cDNA). The AceQ Universal SYBR qPCR Master Mix (Vazyme) was used for qRT-PCR, and the endogenous control mRNA was β-actin.Every sample was examined three times. Each sample's CT (cyclic threshold) value was used to assess the mRNA expression level, and the 2^-ΔΔCT method was used to quantify each sample's relative expression level.

Immunohistochemistry (IHC)

Patients' and naked mice's tissues were preserved with 4% paraformaldehyde, then sectioned, stained, and paraffin embedded (Shangha YiYang Instrument Co., Ltd., Shanghai, China). Immunohistochemical analysis was performed using the Rabbit/Mouse two-step detection kit (Beijing ZSBG-Bio Co., Ltd., Beijing, China) in accordance with the manufacturer's instructions. Immunohistochemical staining was performed using antibodies against YTHDF3 (diluted 1:500; Proteintech, Wuhan, Hubei, P.R.C.; Catalog number: 25537-1-AP), Ki67 (diluted 1:100; Proteintech; Catalog number: 27309-1-AP), and NEK7 (diluted 1:50; Santa Cruz Biotechnology, CA, USA; Catalog number: sc-393539). The average optical density (AOD) method and a double-blind scoring system were used to examine the staining results.

Western blot

Protease/phosphatase inhibitor (Solarbio) and RIPA lysis buffer (Solarbio) were used in a 100:1 ratio to extract the protein. The proteins were moved to a polyvinylidene fluoride membrane (Merck Millipore, Billerica, MA, USA) after being electrophoretically separated on a 10% SDS polyacrylamide gel (Bio-Rad Laboratories Inc., Hercules, CA, USA). In this study, the following antibodies were used: ^{2}-actin antibody (diluted 1:1500; ZSBG-Bio; Catalog number: TA-09), YTHDF3 antibody (diluted 1:1000; Proteintech, Wuhan, Hubei, P.R.C; Catalog number: 25537-1-AP), Cyclin D1 antibody (diluted 1:1000; Proteintech; Catalog number: 60186-1-lg), c-MYC antibody (diluted 1:500; Proteintech; Catalog number: 10828-1AP), Beta Catenin antibody (diluted 1:1000; Proteintech; Catalog number: 51067-2-AP). The Odyssey Scanning System (LI-COR Biosciences, Lincoln, NE, USA) identified the immunoreactive protein bands.

Cell proliferation assay

Each group's cells were evenly spaced in 96-well plates with a density of 2×103 cells per well and cultivated with full culture media for the CCK-8 test. Each well received

10 μL of the Cell Counting Kit -8 (CCK-8; Dojindo, Tokyo, Japan) reagent at 24, 48, 72, and 96 hours following distribution. After that, the cells were kept in the incubator for two more hours. For each well, a Promega GloMax luminescence detector (Promega, Madison, WI, USA) was used to measure the absorbance at 450 nm.

Cells from each group were evenly distributed at a density of 1000 cells per well in 6-well plates for the colony formation test. Every three days, new culture medium was added. After being cultivated for seven to fourteen days, the cells were twice washed with PBS, treated for thirty minutes with 4% paraformaldehyde, then stained for twenty minutes with 0.1% crystal violet.

Cell migration assay

Each group's cells were evenly distributed in 6-well plates for the wound healing test. A 200 μL pipette tip was used to draw two straight lines on each well to represent the wound once the cell confluence reached or was about 100%. Following two PBS washes, the cells were cultivated in a culture medium devoid of FBS.Following the creation of the wound, each well was photographed at 0 and 48 hours. The migration rate was calculated as the ratio of the gap width at 0 to 48 hours.

4×104 (HGC-27, AGS) and 8×104 (MKN7, MKN74) cells were introduced to the upper chamber (Corning Incorporated, Corning, NY, USA) in 200 μLFBS-free media for the Transwell migration test. 700 μL of complete medium was introduced to the lower chamber in order to cause downward migration. Cells on the polycarbonate membrane's upper chamber side were extracted with a swab following a 48-hour culture period. After two PBS cleanings, the chamber was treated for 30 minutes with 4% paraformaldehyde and then for 20 minutes with 0.1% crystal violet. PBS was used one more to clean the extra crystal violet. ImageJ software (National Institutes of Health, Bethesda, MD, USA) was used to count the stained cells after five visual areas were chosen at random for photography.

Cell invasion assay

In order to promote downward invasion of the cells in the upper chamber, cells were resuspended in 100 μL of FBS-free media and introduced to the upper chamber. Meanwhile, 600 μL of complete medium was added to the lower chamber for the Transwell invasion assay. Every other experimental protocol was identical to the Transwell migration assay protocol.

Cell apoptosis assay

48 hours following transfection, cells were extracted from each group and stained with the Annexin V-FITC/PI apoptosis assay kit (NeoBioscience, Shenzhen, China). 1×105 cells were subjected to apoptosis analysis using flow cytometry (BD Biosciences, San Jose, CA, USA), and the percentage of apoptotic cells was determined using FlowJo software.

Animal studies

Ten male BALB/c nude mice weighing 16–20g and 4-6 weeks of age were purchased from Beijing Huafukang Biotechnology Co., LTD. They were split into two groups at random, with five mice in each, and kept in a pathogen-free environment with enough food and water. The room temperature was kept at around 22°C with a light/dark cycle of 12/12 hours. After disinfecting the skin of the nude mice's left anterior axillary fossak, a sterile syringe was used to subcutaneously inject HGC-27 cells (5×106 cells per mouse) that had been stabilized transfected with shRNA-NC and shRNA-YTHDF3. Tumor size was measured every two days beginning on day three after injection using the formula volume = (long diameter × short diameter 2)/2. The naked mice were mercifully put to death when the tumor volume became close to 1000 mm3. After that, the tumor tissues were sectioned and paraffin-embedded for

HE and IHC examination. The aforementioned studies were conducted in compliance with the experimental animal care and use system and authorized by the First Hospital's Ethics Committee at Hebei Medical University.

RNA sequencing (RNA-seq)

After 24 hours of siRNA-NC and siRNA-YTHDF3 transfection, total RNA was collected from HGC-27 cells. Beijing Novogene Technology Co., LTD was given the task of creating the RNA library and conducting the sequencing analysis. Six samples (siNC × 3 and siYTHDF3 × 3) were examined utilizing Illumina's NovaSeq 6000 platform, to put it briefly. To get high-quality data, each sample's output data is subjected to quality control and filtering. High-quality data was aligned to reference genomes using HISAT software, which was also used to measure the sample's levels of gene or transcript expression. Differential genes were classified as those with log2 |Fold Change| > 1.0 and $P < 0.05$. DESeq2 software was utilized for the investigation of differential expression.

Co-Immunofluorescent (Co-IF) assay

In a 6-well plate, HGC-27 cells were uniformly spaced on coverslips. The cells were gently washed three times with PBS once the cell fusion rate had reached 20–30%.The cells were then blocked with 2% bovine serum albumin (BSA-V; Solarbio; Catalog number: A8020), fixed with 4% paraformaldehyde, and penetrated with 0.2% Triton X-10 (Solarbio; Catalog number: T8200). YTHDF3 antibody (diluted 1:50; Proteintech; Catalog number: 25537-1-AP) and NEK7 antibody (diluted 1:50; Santa Cruz Biotechnology; Catalog number: sc-393539) were then added to the cells and incubated for an entire night at 4°C. The cells were then incubated for one hour at room temperature in a dark setting using fluorescent secondary 309 antibody (diluted 1:500; Cy3 anti-rabbit IgG, FITC anti-mouse IgG; Beyotime Biotechnology

Co., Shanghai, China).Lastly, the nuclei were stained with 4'6'-diamino-2-phenylindole dihydrochloride (DAPI; Beyotime Biotechnology Co.). A laser scanning confocal microscope (ZEISS, Oberkochen, Germany) was used to take representative pictures.

Co-immunoprecipitation (Co-IP)

After being extracted, HGC-27 cells were gently given two PBS washes. Following the instructions in the Pierce™ Classic Magnetic IP/Co-IP Kit (Thermo Scientific, Waltham, USA; Catalog number: 88804), cell lysis was then carried out. After lysis, the cell lysate was mixed with 10 μg of the YTHDF3 antibody, 10 μg of the NEK7 antibody, and 10 μg of the IgG antibody from Proteintech. The mixture was then left to incubate for two hours at room temperature. After adding magnetic beads to the lysate, the mixture was constantly spun for an hour at room temperature. Elution Buffer was used to elute the protein after the magnetic beads were separated using a magnetic rack. The pH was brought to a neutral level by adding Neutralization Buffer.Western blot analysis was then performed on the resulting samples.

Bioinformatics analysis

The TCGA (https://www.aclbi.com/static/index.html#/tcga) and GEO (https://www.aclbi.com/static/index.html#/geo) databases were used to determine the expression of YTHDF3 mRNA in the cancer and surrounding tissues of GC patients. Gene expression levels in GC were examined using GEPIA2 (http://gepia2.cancer-pku.cn/#index), along with nearby normal sublocalization within cells. Primers were predicted using PrimerBank (https://pga.mgh.harvard.edu/primerbank/) and the Primer designing tool (https://www.ncbi.nlm.nih.gov/tools/primer-blast/). BioRender

(https://www.biorender.com/) made it easier to create schematic diagrams for scientific purposes.

Statistical analysis

For every experiment group in this investigation, three independent replicates were carried out. Data with a normal distribution were displayed as mean ± standard deviation, whereas data with a non-normal distribution were displayed as median and interquartile distance. SPSS 26.0 (IBM, Armonk, NY, USA) and GraphPad Prism 9.5 (GraphPad Software, La Jolla, CA, USA) were used to perform the statistical analysis in this work. The Student's t-test, one-way ANOVA, and two-way ANOVA were among the statistical techniques used. A P-value of less than 0.05 was deemed statistically significant.

Data Availability

The corresponding author can provide the data produced in this study upon request. The Cancer Genome Atlas (TCGA) and Gene Expression Omnibus (GEO) at GSE54129 and GSE66229 provided the data used in this analysis.

Results

YTHDF3 is upregulated in GC patients and is associated with poor prognosis

To investigate the role of YTHDF3 in the pathophysiology of gastric cancer (GC), we first analyzed its expression in GC and adjacent normal tissues using the TCGA database, as well as the GSE54129 and GSE66229 datasets. Our analysis revealed a significant upregulation of YTHDF3 expression in GC tissues compared to nearby normal tissues (Figure 1A-C). This observation was further supported by the high

expression of YTHDF3 in stomach adenocarcinoma (STAD) tissues as assessed through the GEPIA2 online tool (Figure 1D). Given the limited understanding of YTHDF3's function in GC, we selected it as the target gene for this study. We quantified YTHDF3 mRNA expression in 12 pairs of fresh-frozen GC tissues and adjacent normal tissues using quantitative reverse transcription-polymerase chain reaction (qRT-PCR). The results demonstrated a statistically significant increase in YTHDF3 mRNA expression in GC tissues ($P < 0.01$), consistent with the TCGA and GEO data (Figure 1E). To validate these findings at the protein level, we performed immunohistochemistry (IHC) on the GC and adjacent normal tissue. The IHC results showed that YTHDF3 protein was predominantly localized in the cytoplasm of GC cells and was significantly overexpressed in GC tissues compared to adjacent normal tissues ($P < 0.001$, x2 = 12.19) (Figure 1F, Table 1). Subsequently, we explored the relationship between YTHDF3 expression and the clinical characteristics of GC patients. The expression of YTHDF3 was found to be independent of gender, age, tumor size, and tumor differentiation. However, it was significantly associated with lymph node metastasis ($P < 0.01$) and TNM staging ($P < 0.05$) (Table 2). These data suggest that YTHDF3 overexpression is linked to a poor prognosis in GC patients, highlighting its potential as a significant biomarker and therapeutic target in GC.

Knockdown of YTHDF3 suppresses proliferation, migration, and invasion and promotes the apoptosis of GC cells *in vitro*

We first downregulated YTHDF3 expression in HGC-27 and AGS cell lines and examined the impact on several cellular processes in order to investigate the mechanism of YTHDF3 in GC. There was a considerable decrease in YTHDF3's mRNA (Figure 2A, B) and protein (Figure 2C, D) levels after transfection with siRNA targeting YTHDF3 (siYTHDF3) and a siRNA negative control (siNC). The The CCK-8 experiment demonstrated that the cell viability in HGC-27 and AGS cells

was significantly reduced following YTHDF3 knockdown when compared to the control group(Figure 2E, F). The wound healing capacity of YTHDF3 knockdown cells was significantly impaired compared to the control group in both HGC-27 and AGS cells after 48 hours(Figure 2G, H). The number of apoptotic cells in HGC-27 and AGS cell lines increased when YTHDF3 expression was silenced, as indicated by flow cytometry analysis(Figure 2I, J). Furthermore, the Transwell assay results indicated a significant reduction in both the number of migrated and invasive cells in the YTHDF3 knockdown group for both HGC-27 and AGS cell lines(Figure 2K, L, M, N). These findings imply that YTHDF3 downregulation stimulates apoptosis and suppresses GC cell invasion, migration, and proliferation.

The overexpression of YTHDF3 promotes the proliferation, migration, and invasion and suppresses the apoptosis of GC cells *in vitro*

We upregulated YTHDF3 expression in MKN7 and MKN74 cell lines to observe its impact on cellular biological functions. Following transfection of the cells with pcDNA3.1-YTHDF3 (YTHDF3) and pcDNA3.1-vector (Vector), we observed a marked increase in YTHDF3 mRNA (Figure 3A, B) and protein (Figure 3C, D) levels. The CCK-8 assay revealed a significant enhancement in cell viability in MKN7 and MKN74 cells upon YTHDF3 overexpression, as compared to the control group (Figure 3E, F). The wound healing ability of cells with YTHDF3 upregulation was significantly enhanced compared to the control group in both MKN7 and MKN74 cells after 48 hours(Figure 3G, H). The number of apoptotic cells in the MKN7 and MKN74 cell lines increased when YTHDF3 expression was elevated, according to the flow cytometry study (Figure 3I, J).Furthermore, the Transwell assay results demonstrated a significant increase in both the number of migrated and invasive cells in the YTHDF3-upregulated group for both the MKN7 and MKN74 cell lines(Figure 3K, L, M, N). In conclusion, our findings imply that YTHDF3 may function as a pro-oncogene in GC as overexpression of the protein can increase GC cell invasion, migration, and proliferation while preventing apoptosis.

YTHDF3 deficiency inhibits the growth of GC *in vivo*

We created tumor-bearing nude mouse models with reduced YTHDF3 expression and equivalent negative controls in order to better understand the mechanism of YTHDF3 in GC *in vivo*. After successfully establishing HGC-27 cell lines that were stably transfected with shRNA-YTHDF3 and shRNA-negative control (shNC/shYTHDF3), the cells were subcutaneously injected into two groups of naked mice, respectively. Figure 4A-D displayed the tumor-bearing models as well as the tumor volume curves, tumor photos, and tumor weights. The growth rate, volume, and weight of tumors in the shYTHDF3 group were significantly lower than those in the shNC group, according to the results. The xenograft tissues' morphological features were assessed by HE staining, and the findings showed that the cell structure and morphology resembled those of GC tissues (Figure 4E). When compared to the shNC group, the proliferation ability of cells in the shYTHDF3 group was greatly suppressed, according to Ki67 immunohistochemical staining (Figure 4F). These results imply that GC growth can be inhibited in vivo by YTHDF3 knockdown.

NEK7 is the potential target of YTHDF3 in GC

We conducted RNA-seq in HGC-27 cells of the siNC group and the siYTHDF3 group, respectively, to better investigate the possible role of YTHDF3 in the pathophysiology of GC. According to the RNA-seq results, YTHDF3 expression knockdown significantly altered the expression levels of 5672 genes in total, including both up-regulated and down-regulated genes (Figure 5A, B). Through the analysis of down-regulated genes identified by RNA-seq(fold change>2 and $P<0.05$), along with the top 1000 genes co-expressed with YTHDF3 in gastric cancer samples from the TCGA database, and the 3742 genes that are highly expressed in gastric cancer within the same database, two genes were identified as potential candidates for binding to the

YTHDF3 protein. These two genes (NEK7/MPZL1) were shown to be potential target genes for YTHDF3 (Figure 5C). Subsequent analysis of these genes involved examining their subcellular distribution, expression levels in gastric cancer tissues, and the survival outcomes of patients with gastric cancer associated with these genes. Data from the TCGA database revealed that NEK7 was prominently expressed in gastric cancer tissues (Figure 5D), predominantly localized to the cytoplasm and nucleus (Figure 5E). Moreover, patients exhibiting high levels of NEK7 expression exhibited significantly reduced overall survival rates (Figure 5F). Therefore, we speculate that NEK7 is a potential downstream target gene. Co-IF and Co-IP tests were then used to confirm the interaction between YTHDF3 and NEK7. The Co-IF results demonstrated that YTHDF3 and NEK7 co-localize and are primarily found in the cytoplasm and nucleus of GC cells (Figure 5G). YTHDF3 and NEK7 can co-precipitate in GC cells, according to the Co-IP data (Figure 5H). Lastly, we investigated the transcriptional and translational alterations of NEK7 following YTHDF3 knockdown or overexpression in order to further validate the control of NEK7 expression by YTHDF3 in GC cells. After down-regulating YTHDF3 expression in HGC-27 cells, both NEK7 mRNA and protein expression were reduced (Figures 5I, J). Similarly, when YTHDF3 expression was upregulated in MKN74 cells, both NEK7 mRNA and protein expression levels were increased (Figures 5K, L). These events suggest that YTHDF3 controls downstream gene expression at both the transcriptional and translational levels. In summary, these findings indicate an interaction between YTHDF3 and NEK7 in gastric cancer, and that YTHDF3 can regulate the production of NEK7 protein. NEK7 may serve as a potential modification target of YTHDF3 in gastric cancer.

NEK7 is highly expressed in GC and interacts with YTHDF3

Next, we first confirmed that GC cell lines and GC tissues expressed NEK7.According to the findings, GC cell lines had a greater level of NEK7 mRNA than normal gastric mucosa cells (Figure 6A), and GC tissues had a higher level of NEK7 mRNA in adjacent tissues (18 pairs of GC paired tissues) (Figure 6B). MKN74

cells had the highest NEK7 protein expression (Figure 6C), while GC tissues had higher levels than nearby tissues (44 pairs of GC paired tissues) (Figure 6D). These findings imply that NEK7 might have a role in GC pathogenesis as an oncogene. Subsequently, we aim to further elucidate the mechanism by which the interaction between YTHDF3 and NEK7 contributes to the development of gastric cancer. One of the siRNA sequences with the greatest knockdown efficacy (si-NEK7-659) was selected for further testing after four siRNA-NEK7 sequences were transfected concurrently into MKN74 cells with the highest NEK7 expression (Figure 6E-F). We then transfected siRNA-negative control/siRNA-YTHDF3 and pcDNA3.1-vector/pcDNA3.1-NEK7 into HGC-27 and siRNA-negative control/siRNA-NEK7 and pcDNA3.1-vector/pcDNA3.1-YTHDF3 into MKN74 cells, either simultaneously or separately. qRT-PCR and Western blot were used to identify the variations in YTHDF3 expression in each group. The findings imply that NEK7 overexpression may mitigate the knockdown effect of YTHDF3 in HGC-27 cells (Figure 6J-H), while NEK7 knockdown may also mitigate the up-regulation effect of YTHDF3 in MKN74 cells (Figure 6I-J). These results suggest that NEK7 can influence GC cells' YTHDF3 expression.

YTHDF3 targets NEK7 to activate the Wnt/β-catenin signaling pathway in cancer promotion.

We performed KEGG pathway enrichment analysis on the list of differentially expressed genes found in RNA-seq data and examined the signaling pathways regulated by them in order to elucidate the oncogenic mechanism of YTHDF3 in gastric cancer. The findings indicated a high enrichment of genes in the Wnt/β-catenin signaling pathway (Figure 7A).We then investigated whether NEK7 might reverse the inhibitory effects of YTHDF knockdown on the activation of the Wnt/β-catenin signaling pathway. The findings imply that downstream effectors of β-catenin (c-MYC, CD1) similarly exhibit markedly decreased expression levels in HGC-27 cells when YTHDF3 expression is downregulated. At the same time, NEK7

overexpression can reverse the downregulation of these effectors brought on by YTHDF3 knockdown (Figure 7B). These results imply that YTHDF3 regulates the activation of the Wnt/β-catenin signaling pathway via NEK7. We then investigated whether NEK7 would have an impact on YTHDF3's effects on GC cell function. The findings demonstrated that the up-regulation of NEK7 expression could recover the attenuation of cell proliferation, migration, and invasion in HGC-27 cells caused by YTHDF3 knockdown (Figure 7C-G). The down-regulation of NEK7 expression may mitigate the augmentation of cell proliferation, migration, and invasion brought on by YTHDF3 overexpression in MKN74 cells (Figure 7D-L). In conclusion, NEK7 is an essential downstream target for YTHDF3 that aids in the development of GC, and NEK7 and the cGMP-PKG signaling pathway are necessary for YTHDF3 to have an oncogenic effect in GC. As a result, we suggest that elevated YTHDF3 may enhance the production of the NEK7 mRNA and protein, which in turn may activate the Wnt/β-catenin signaling pathway and eventually encourage the development of tumors in GC cells.

Discussion

This study reveals that YTHDF3 is significantly upregulated in gastric cancer (GC) patients and is closely associated with poor prognosis. In both in vitro and in vivo models, YTHDF3 exhibits characteristics of an oncogene. Knockdown of YTHDF3 markedly inhibits the proliferation, migration, and invasion of GC cells while promoting apoptosis, whereas overexpression of YTHDF3 has the opposite effect. Further research indicates that YTHDF3 exerts its oncogenic role by targeting NEK7 and activating the Wnt/β-catenin signaling pathway, suggesting that YTHDF3 may promote tumor development in GC cells by enhancing the production of NEK7 mRNA and protein.

Previous studies have found that YTHDF3 expression was significantly higher in HCC tissues than in paracancerous liver tissues. YTHDF3 was also significantly upregulated in HCC with microvascular invasion (MVI) compared to that in HCC without MVI [19]. This is consistent with our findings of elevated YTHDF3 mRNA and protein expression levels in GC tissues. Further analysis of the relationship between YTHDF3 expression and clinical pathological data in GC patients revealed that high YTHDF3 expression is closely associated with lymph node metastasis and more advanced TNM stages, which holds significant value for individualized clinical treatment and prognostic assessment.

To validate the impact of YTHDF3 on the biological functions of GC cells, our experiments demonstrated that knockdown of YTHDF3 in GC cells significantly suppressed cell proliferation, migration, and invasion, and increased apoptosis. Conversely, upregulation of YTHDF3 in GC cells produced the opposite effects. Moreover, in vivo experiments in nude mice showed that YTHDF3 depletion inhibited the growth of gastric tumors. Reports have indicated that YTHDF3 overexpression facilitated the proliferation, invasion, and migration of HCC cells both in vitro and in vivo. However, the YTHDF3 knockdown resulted in an inverse trend. [17]. YTHDF3 is required for the maintenance of CSC properties and tumor initiation capacity in ocular melanoma both in vitro and in vivo. Ocular melanoma cells with targeted YTHDF3 knockdown exhibited inhibitory tumor proliferation and migration abilities[13]. This aligns with our findings, collectively confirming that YTHDF3 may facilitate malignant biological characteristics such as growth and metastasis, potentially contributing to the development of gastric cancer.

Subsequently, we sought to identify the target genes mediating YTHDF3's effects to elucidate the molecular mechanisms of GC. Through RNA-seq, downregulated gene analysis, YTHDF3 correlation analysis, and STAD-DEGs-up gene overlap analysis, combined with online database analysis and literature review, we found that NEK7 drew our attention. We confirmed its binding to YTHDF3 through

co-immunoprecipitation followed by Western blotting. Confocal immunofluorescence experiments and immunoprecipitation further confirmed the interaction between YTHDF3 and NEK7 in GC cells, a finding not previously reported. NEK7 is a multifunctional serine/threonine kinase expressed in various organs and is crucial for cell division, mitochondrial function, and protein transport. Studies have shown that NEK7 is highly expressed in multiple cancers and is closely associated with tumor growth, invasion, and metastasis [19]. In particular, the role of NEK7 has been confirmed in retinoblastoma, breast cancer, hepatocellular carcinoma, and pancreatic cancer [20-22]. Fortunately, these results are consistent with our current findings on NEK7 in gastric cancer. To explore the mechanism by which YTHDF3 regulates NEK7 in gastric cancer, we demonstrated that YTHDF3 regulates NEK7 expression at the translational level and the transcriptional level. Therefore, YTHDF3 may bind to NEK7 mRNA and promote its translation, ultimately leading to the progression of gastric cancer.

Enrichment analysis of differentially expressed genes from RNA-seq in the KEGG pathway revealed significant enrichment in the Wnt/β-catenin signaling pathway. The classic WNT/β-catenin signaling pathway maintains high stability during evolution and plays a key regulatory role in tissue formation and homeostasis [23]. This pathway plays a central role in cancer formation, progression, and immune therapy responses. Under normal physiological conditions, it is responsible for regulating cell growth, differentiation, and programmed cell death; however, in cancer cells, its overactivation typically promotes tumor growth and spread, and helps tumor cells evade immune surveillance. Numerous studies have shown that Wnt signaling pathway-related proteins are widely distributed in various types of cancer, such as colorectal cancer [24], lung cancer [25], malignant melanoma [26], breast cancer [27], hepatocellular carcinoma [28], and pancreatic cancer [29]. These proteins are foundin the membrane structures, cytoplasm, and nuclei of tumor cells. Clearly, the Wnt/β-catenin pathway plays a dominant role in the initiation and evolution of cancer, driving the occurrence and malignant transformation of cancer cells [30,31]. Based on

the above analysis, we hypothesized that high YTHDF3 expression may promote the oncogenic effects of the Wnt/β-catenin signaling pathway. Subsequently, we used Western blotting to detect key markers of the Wnt/β-catenin pathway, including β-Catenin, c-MYC, and CD1. We found that the inhibitory effect of YTHDF3 knockdown on Wnt/β-catenin pathway activation could be rescued by NEK7 overexpression, and NEK7 itself was capable of activating the Wnt/β-catenin signaling pathway. In subsequent rescue experiments, we further confirmed that the YTHDF3/NEK7/Wnt/β-catenin axis affects the growth, migration, and invasion capabilities of GC cells. These results suggest that the YTHDF3/NEK7/Wnt/β-catenin axis is involved in the occurrence and development of gastric cancer, providing potential molecular targets for the diagnosis and treatment of gastric cancer, and laying the foundation for further research on the role of the YTHDF family in cancer development.

However, this study has some limitations that need to be addressed in future research. For example, while this study focused primarily on the Wnt/β-catenin signaling pathway, YTHDF3-mediated proliferation, migration, and invasion of GC cells may also involve other signaling pathways. The roles and interactions of these pathways require further investigation. This study proposes targeting YTHDF3 as a potential therapeutic strategy for gastric cancer but did not conduct specific drug intervention studies. Future research needs to develop inhibitors targeting YTHDF3 and test their efficacy in vitro and in vivo models.

In conclusion, this study reveals the important role of YTHDF3 in the proliferation, migration, and invasion of gastric cancer cells and is the first to confirm its molecular mechanism of promoting gastric cancer progression by interacting with NEK7 and activating the Wnt/β-catenin signaling pathway. This provides new molecular targets for the diagnosis and treatment of gastric cancer, contributes to a deeper understanding of the role of the YTHDF family in cancer development, and confirms the key role of the Wnt/β-catenin signaling pathway in the progression of gastric

cancer, providing a theoretical basis for targeted therapeutic strategies against this pathway.

Acknowledgments

This work was supported by Hebei Provincial Government-funded Provincial Medical Excellent Talent Project (ZF2023025, ZF2024134, ZF2025045, ZF2025048, ZF2025051, ZF2025271, LS202208 and LS202212), Hebei Natural Science Foundation (H2022206292, H2024206140), Key R&D Program of Hebei Province (223777103D and 223777113D), Hebei Province County General Hospital Appropriate Health Technology Promotion Project (20220018), Prevention and treatment of geriatric diseases by Hebei Provincial Department of Finance (LNB202202, LNB201809 and LNB201909), Spark Scientific Research Project of the First Hospital of Hebei Medical University (XH202312 and XH201805), Hebei Province Medical Applicable Technology Tracking Project (G2019035) and other projects of Hebei Province (1387 and SGH201501).

References

1. Bray F, Ferlay J, Soerjomataram I, et al. Global cancer statistics 2022: GLOBOCAN estimates of incidence and mortality worldwide for 36 cancers in 185 countries. CA Cancer J Clin. 2024 May-Jun;74(3):229-263.

2. Zaccara S, Patil DP, Jaffrey SR. A unified model for the function of YTHDF proteins in regulating m6A-modified mRNA. Cell. 2020;181:1582-1595.

3. Li L, Tang C, Ye J, et al. Bioinformatic analysis of m6A “reader” YTH family in pan-cancer as a clinical prognosis biomarker. Sci Rep. 2023;13:17350.

4. Mei Z, Shen Z, Pu J, et al. NAT10 mediated ac4C acetylation driven m6A modification via involvement of YTHDC1-LDHA/PFKM regulates glycolysis and promotes osteosarcoma. Cell Commun Signal. 2024;22:51.

5. Liao Y, Liu Y, Yu C, et al. HSP90β impedes STUB1-induced ubiquitination of

YTHDF2 to drive sorafenib resistance in hepatocellular carcinoma. Adv Sci. 2023;10:e2302025.

6. Song JK, You GH, Yin XH, et al. Overexpression of YTHDC2 contributes to the progression of prostate cancer and predicts poor outcomes in patients with prostate cancer. J Biochem Mol Toxicol. 2023;37:e23308.

7. Chen J, Sun Y, Xu X, et al. YTH domain family 2 orchestrates epithelial-mesenchymal transition/ proliferation dichotomy in pancreatic cancer cells. Cell Cycle. 2017;16:2259-2271.

8. Song P, Li X, Chen S, et al. YTHDF1 mediates N-methyl-N-nitrosourea-induced gastric carcinogenesis by controlling HSPH1 translation. Cell Prolif. 2024;57:e13619.

9. Sheng H, Li Z, Su SX, et al. YTH domain family 2 promotes lung cancer cell growth by facilitating 6-phosphogluconate dehydrogenase mRNA translation. Carcinogenesis. 2020;41(5):541-550.

10. Li J, Ahmad M, Sang L, et al. O-GlcNAcylation promotes the cytosolic localization of the m6A reader YTHDF1 and colorectal cancer tumorigenesis. J Biol Chem. 2023;299:104738.

11. Ries RJ, Zaccara S, Klein P, et al. m6A enhances the phase separation potential of mRNA. Nature. 2019;571:424-428.

12. Lin Y, Chen X, Huang Y, et al. YTHDF3 facilitates triple-negative breast cancer progression and metastasis by stabilizing ZEB1 mRNA in an m6A-dependent manner. Ann Transl Med. 2022 Jan;10(2):83.

13. Xu Y, He X, Wang S. The m6A reading protein YTHDF3 potentiates tumorigenicity of cancer stem-like cells in ocular melanoma through facilitating CTNNB1 translation. Oncogene. 2022;41(9):1281-1297.

14. Liu D, Li Z, Zhang K, et al. N-methyladenosine reader YTHDF3 contributes to the aerobic glycolysis of osteosarcoma through stabilizing PGK1 stability. J Cancer Res Clin Oncol.

15. Ni W, Yao S, Zhou Y, et al. Long noncoding rna Gas5 inhibits progression of colorectal cancer by interacting with and triggering yap phosphorylation and degradation and is negatively regulated by the M6A reader Ythdf3. Mol Cancer.

2019;18(1):143.

16. Hu Y, Zhang Y, Chen X, et al. A reciprocal feedback between N6-methyladenosine reader YTHDF3 and lncRNA DICER1-AS1 promotes glycolysis of pancreatic cancer through inhibiting maturation of miR-5586-5p. J EXP Clin Cancer Res. 2022 Feb 19;41(1):69.

17. Hu B, Gao J, et al. m6A reader YTHDF3 triggers the progression of hepatocellular carcinoma through the YTHDF3/m6A-EGFR/STAT3 axis and EMT. Mol Carcinog. 2023 Jul 14;62(10):1599-1614.

18. Zhao Y, Zhang Y, Li Y, et al. YTHDF3 Facilitates eIF2AK2 and eIF3A Recruitment on mRNAs to Regulate Translational Processes in Oxaliplatin-Resistant Colorectal Cancer. ACS Chemical Biology. 2022 Jul 15;17(7):1778-1788.

19. Eisa NH, Jilani Y, Kainth K, et al. The co-chaperone UNC45A is essential for the expression of mitotic kinase NEK7 and tumorigenesis. J Biol Chem. 2019;294:5246-5260.

20. Kooi IE, Mol BM, Massink MP, et al. A Meta-Analysis of Retinoblastoma Copy Numbers Refines the List of Possible Driver Genes Involved in Tumor Progression. PLoS One. 2016;11(4):e0153323.

21. Zhang J, Wang L, Zhang Y. Downregulation of NIMA-related kinase-7 inhibits cell proliferation by inducing cell cycle arrest in human retinoblastoma cells. Exp Ther Med. 2018;15(2):1360-1366.

22. Yan Z, Qu J, Li Z, et al. NEK7 Promotes Pancreatic Cancer Progression And Its Expression Is Correlated With Poor Prognosis. Front Oncol. 2021;11:705797.

23. Liu D, Chen L, Zhao H, et al. Small molecules from natural products targeting the Wnt/beta-catenin pathway as a therapeutic strategy. Biomed Pharmacother. 2019;117:108990.

24. O'Brien CA, Pollett A, Gallinger S, et al. A human colon cancer cell capable of initiating tumour growth in immunodeficient mice. Nature. 2007;445(7123):106-10.

25. Pan JC, Fang S, Tian HH. lncRNA JPX/miR-33a-5p/Twist1 axis regulates tumorigenesis and metastasis of lung cancer by activating Wnt/β-catenin signaling. Mol Cancer. 2020;19(1):9.

26. Dong F, Nguyen T, Kim L, et al. A tumorigenic subpopulation with stem cell properties in melanomas. Cancer Res. 2005;65(20).

27. Chen ZH, Tian Y. CMTM7 inhibits breast cancer progression by regulating Wnt/β-catenin signaling. Breast Cancer Res. 2023;25(1):22.

28. Ma S, Chan KW, Hu L, et al. Identification and characterization of tumorigenic liver cancer stem/progenitor cells. Gastroenterology. 2007;132(7):2542-56.

29. He JL, Yang GH, Cao RL, et al. RGC-32 facilitates pancreatic cancer via activating Wnt/β-catenin signaling. Cell Mol Biol. 2023;69(14):161-165.

30. Verras M, Sun Z. Roles and regulation of Wnt signaling and beta-catenin in prostate cancer. Cancer Lett. 2006;237(1).

31. Wend P, Holland JD, Ziebold U, et al. Wnt signaling in stem and cancer stem cells. Semin Cell Dev Biol. 2010;21(8).

Table 1 The expression level of YTHDF3 protein in two groups

Group	Cases	YTHDF3 expression		High Rate(%)	χ^2	*P*
		High	Low			
Gastric cancer tissues	50	28	22	56	15.48	< 0.001***
Adjacent normal tissues	50	9	41	18		

Table 2 The relationship between the expression of YTHDF3 in gastric cancer tissue and the clinicoapathological data of patients

Group	Cases	YTHDF3 expression		χ^2	*P*
		High	Low		
Gender					
Male	37	20	17	0.219	0.64
Female	13	8	5		
Age (years)					
≦60	11	5	6	0.636	0.425
＞60	39	23	16		
Tumor size (cm)					
≦4 cm	27	15	12	0.005	0.945
＞4 cm	23	13	10		
Differentiation					
Poorly	26	14	12	0.102	0.749
Well	24	14	10		
Lymphnode metastasis					
Absent	16	5	11	5.850	0.016**
Present	34	23	11		
TNM Staging					
I＋II	21	8	13	4.711	0.030*
III＋IV	29	20	9		

Figure 1

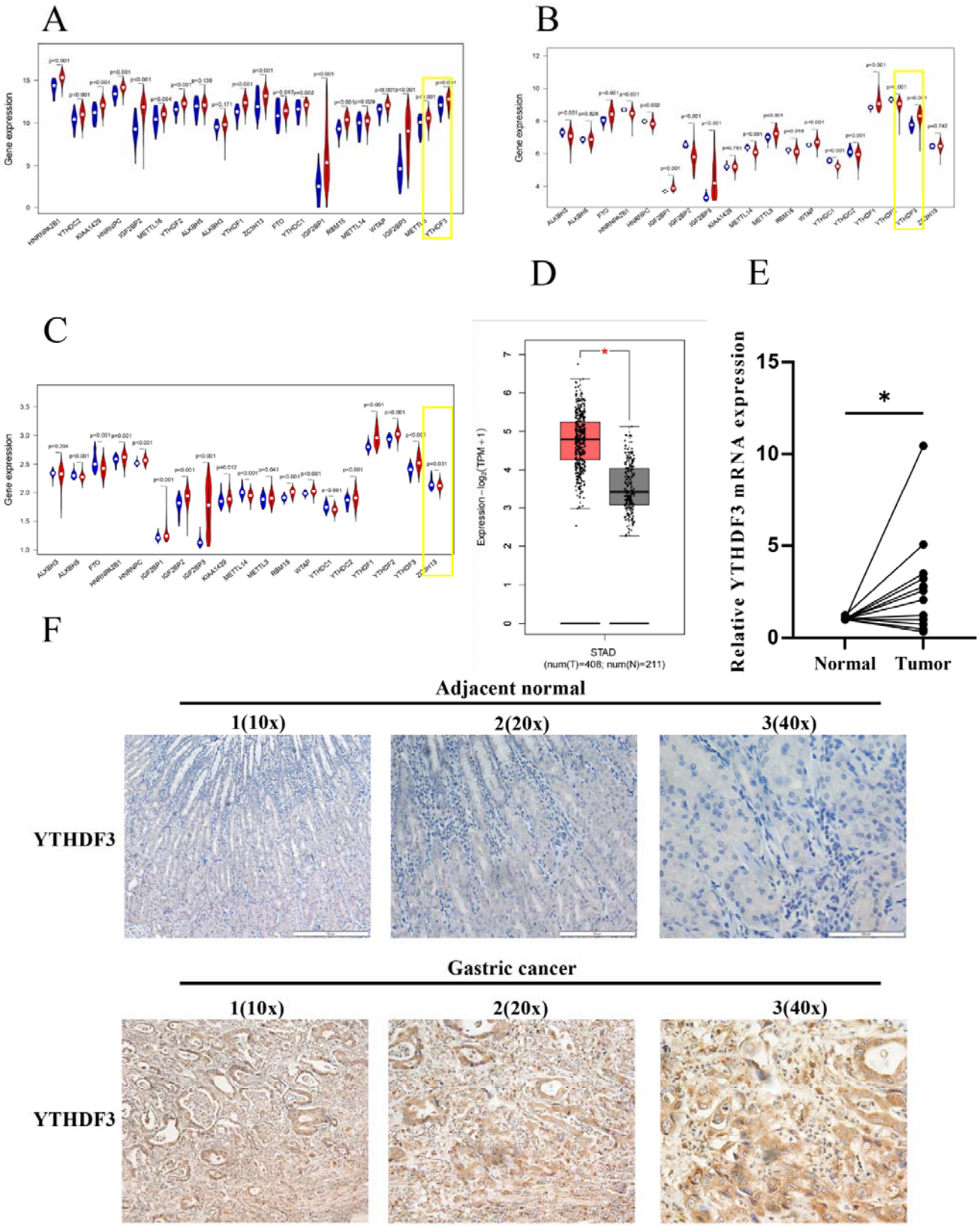
A
B
C
D
E
F
Gene expression
Expression – log2(TPM + 1)
STAD
(num(T)=408; num(N)=211)
Relative YTHDF3 mRNA expression
Normal
Tumor
Adjacent normal
1(10x)
2(20x)
3(40x)
YTHDF3
Gastric cancer
1(10x)
2(20x)
3(40x)
YTHDF3

Figure 1. Increased YTHDF3 expression is associated with poor prognosis in GC patients. (A-C) Expression of YTHDF3 in the TCGA database, as well as the GSE54129 and GSE66229 datasets. **(D)** YTHDF3 is highly expressed in STAD tissues through the analysis of the online databases GEPIA2. **(E)** The expression levels of YTHDF3 mRNA in 12 pairs of GC and adjacent normal tissue samples were detected by qRT-PCR. **(F)** Representative images showing YTHDF3 protein expression levels in 50 pairs of GC and adjacent normal tissue samples, as detected by IHC. Scale bar, 20 μm. Data are presented as means ± SD. *P <0.05

Figure 2

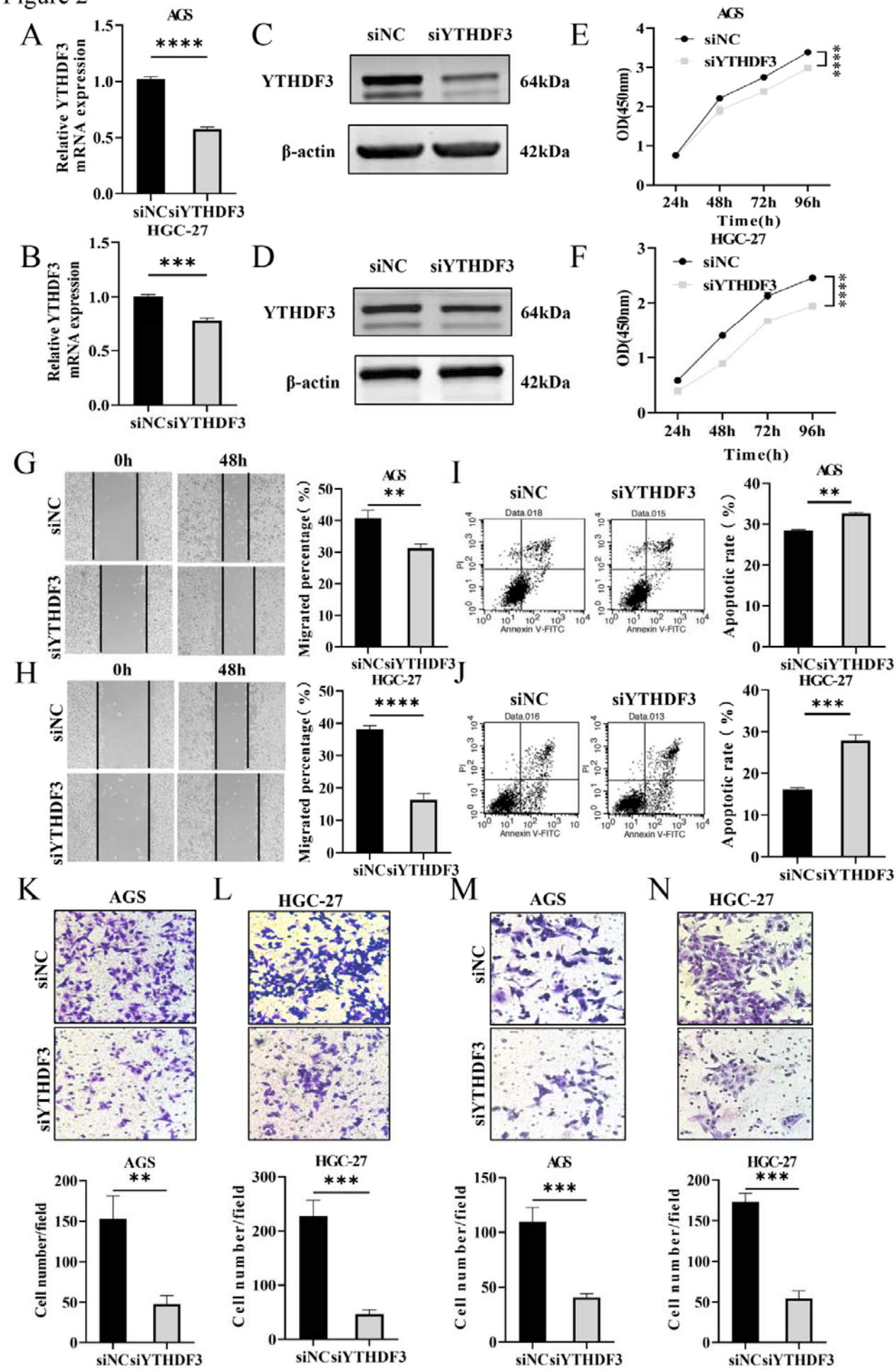
A
AGS
****
Relative YTHDF3 mRNA expression
siNC siYTHDF3
B
HGC-27
***
C
siNC siYTHDF3
YTHDF3
64kDa
β-actin
42kDa
D
E
OD(450nm)
Time(h)
24h 48h 72h 96h
F
G
0h
48h
siNC
siYTHDF3
Migrated percentage (%)
H
I
Apoptotic rate (%)
J
K
L
M
N
Cell number/field

Figure 2. Knockdown of YTHDF3 in GC cells suppresses cell proliferation, migration and invasion *in vitro*. (A, B) The expression of YTHDF3 mRNA in HGC-27 and AGS cells was detected by qRT-PCR. **(C, D)** The expression of YTHDF3 protein in HGC-27 and AGS was detected by WB. **(E, F)** The effect of YTHDF3 knockdown on the proliferation of HGC-27 and AGS cells was determined by the CCK-8 assay. **(G, H)** The effect of YTHDF3 knockdown on the migration of HGC-27 and AGS cells was assessed by the wound healing assay. Scale bar, 200 μm. **(K, L)** The effect of YTHDF3 knockdown on the migration of HGC-27 and AGS cells was evaluated using the Transwell migration assay. Scale bar, 100 μm. **(M, N)** The effect of YTHDF3 knockdown on the invasion of HGC-27 and AGS cells was assessed using Transwell invasion assay. Scale bar, 100 μm. **(I, J)** The effect of YTHDF3 knockdown on the apoptosis of HGC-27 and AGS cells was determined by flow cytometry. Data are presented as means ± SD. $^{*}P<0.05$, $^{**}P<0.01$, $^{***}P<0.001$, $^{****}P<0.0001$

Figure3

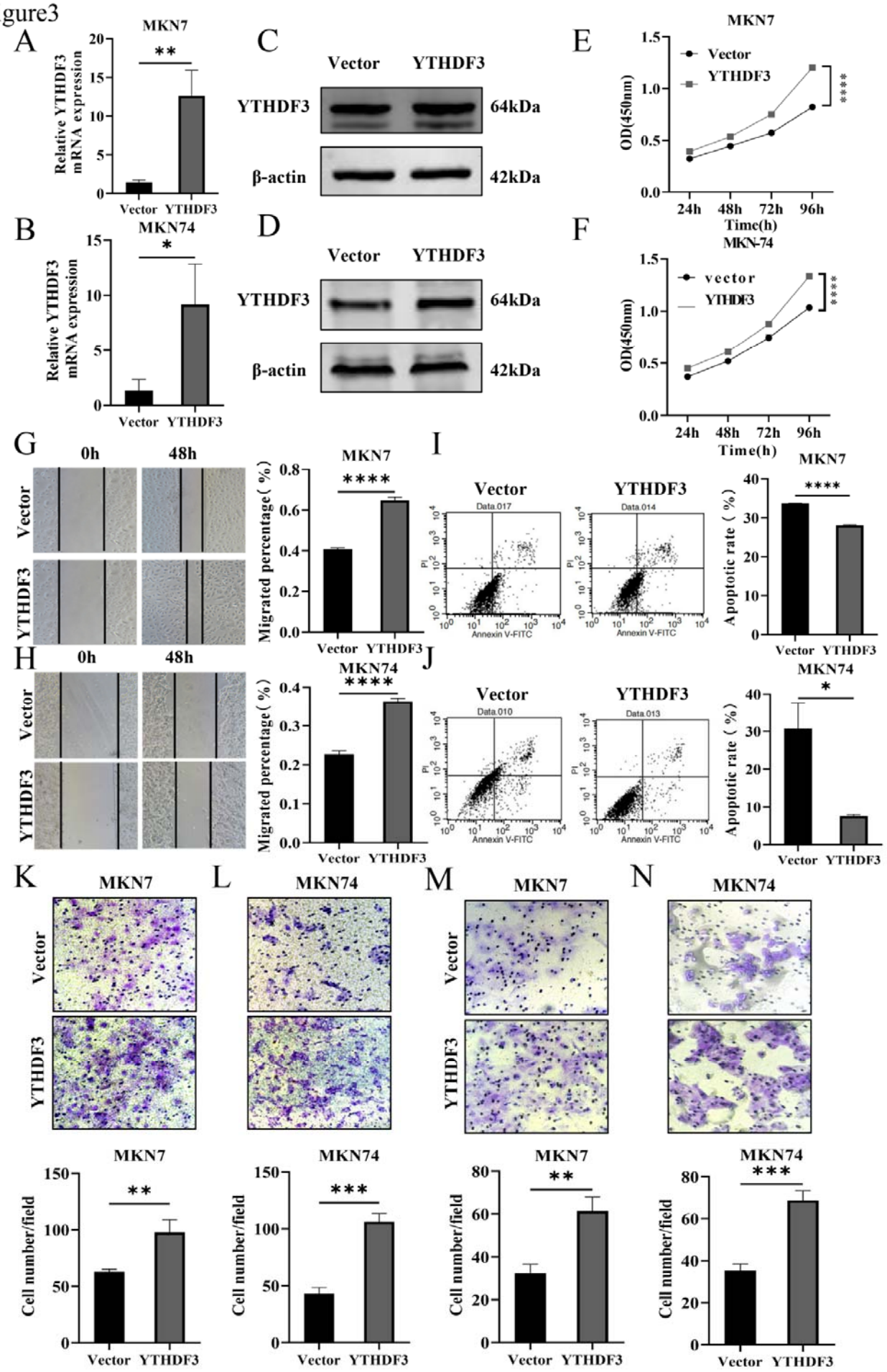
A
MKN7
Relative YTHDF3 mRNA expression
Vector
YTHDF3
B
MKN74
C
Vector
YTHDF3
64kDa
β-actin
42kDa
D
E
MKN7
OD(450nm)
Time(h)
24h
48h
72h
96h
F
MKN-74
vector
G
0h
48h
Migrated percentage(%)
H
I
Apoptotic rate (%)
Annexin V-FITC
PI
J
K
L
M
N
Cell number/field

Figure 3. Overexpression of YTHDF3 in GC cells and human gastric mucosa cells promotes cell proliferation, migration and invasion i*n vitro*. (A, B) The expression of YTHDF3 mRNA in MKN7 and MKN74 was detected by qRT-PCR. **(C, D)** The expression of YTHDF3 protein in MKN7 and MKN74 was detected by WB. **(E, F)** The effect of YTHDF3 overexpression on the proliferation of MKN7 and MKN74 cells was assessed using the CCK-8 assay. **(G, H)** The effect of YTHDF3 overexpression on the migration of MKN7 and MKN74 cells was evaluated through a wound healing assay. Scale bar, 200 μm. **(K, L)** The effect of YTHDF3 overexpression on the migration of MKN7 and MKN74 cells was determined utilizing a Transwell migration assay. Scale bar, 100 μm. **(M, N)** The effect of YTHDF3 overexpression on the invasion of MKN7 and MKN74 cells was assessed via a Transwell invasion assay. Scale bar, 100 μm. **(I, J)** The effect of YTHDF3 overexpression on the apoptosis of MKN7 and MKN74 cells was analyzed by flow cytometry. Data are presented as means ± SD. $^{**}P < 0.01$, $^{***}P < 0.001$, $^{****}P < 0.0001$

Figure 4

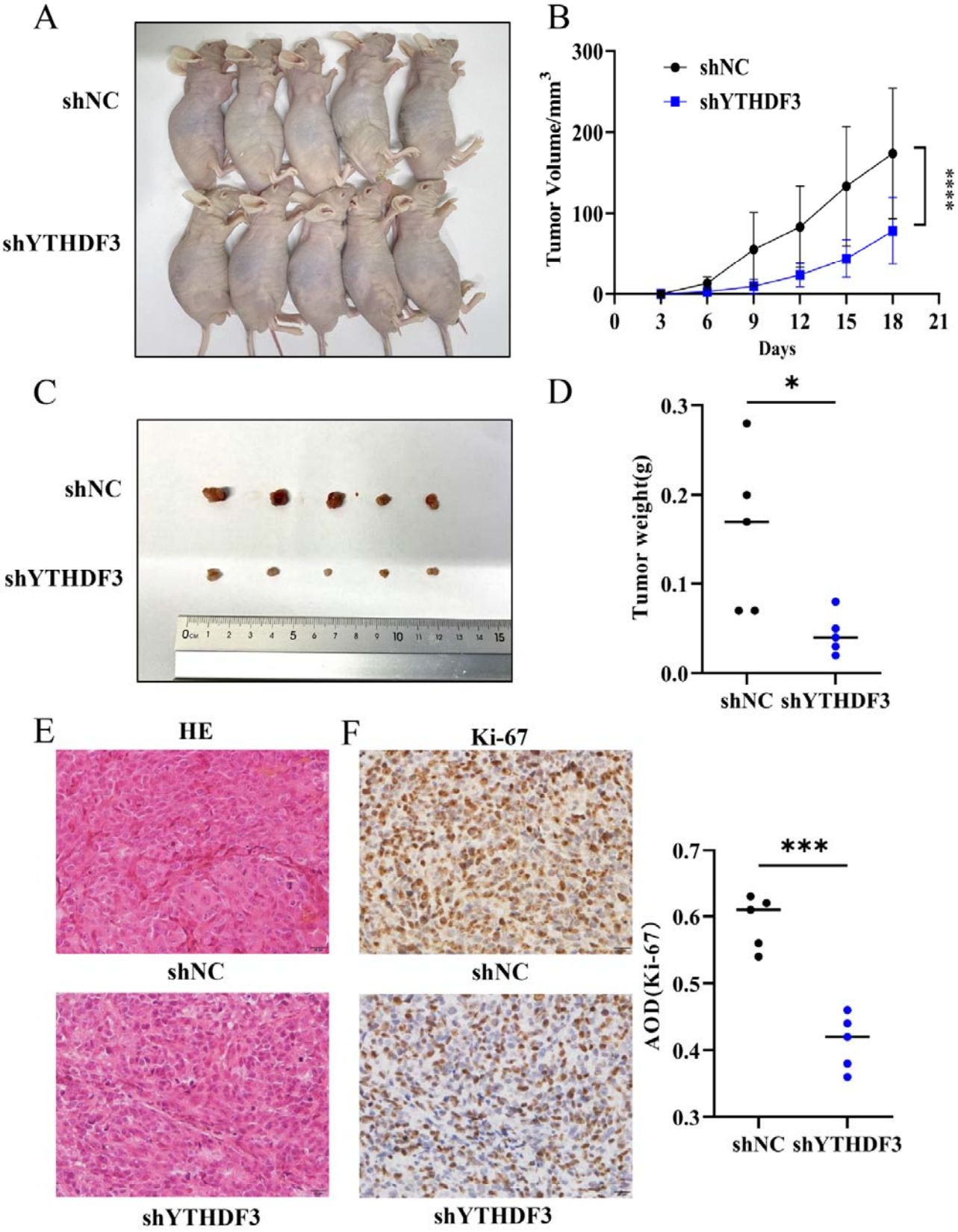
A
shNC
shYTHDF3
B
shNC
shYTHDF3
Tumor Volume/mm3
300
200
100
0
0 3 6 9 12 15 18 21
Days
****
C
shNC
shYTHDF3
D
*
Tumor weight(g)
0.3
0.2
0.1
0.0
shNC shYTHDF3
E
HE
shNC
shYTHDF3
F
Ki-67
shNC
shYTHDF3
***
AOD(Ki-67)
0.7
0.6
0.5
0.4
0.3
shNC shYTHDF3

Figure 4. YTHDF3 regulates the growth of GC *in vivo*. (A) Nude mouse tumor-bearing model. **(B)** Tumor growth curve. **(C, D)** Images (C) and weight (D) of xenografted tumors were analyzed. **(E)** Representative images of tumor tissue sectionsstained with HE. Scale bar, 50 μm. **(F)** Representative image of Ki67 IHC staining in tumor tissue sections. Scale bar, 50 μm. Data are shown as means ± SD. $^{*}P < 0.05$, $^{***}P < 0.001$

Figure5

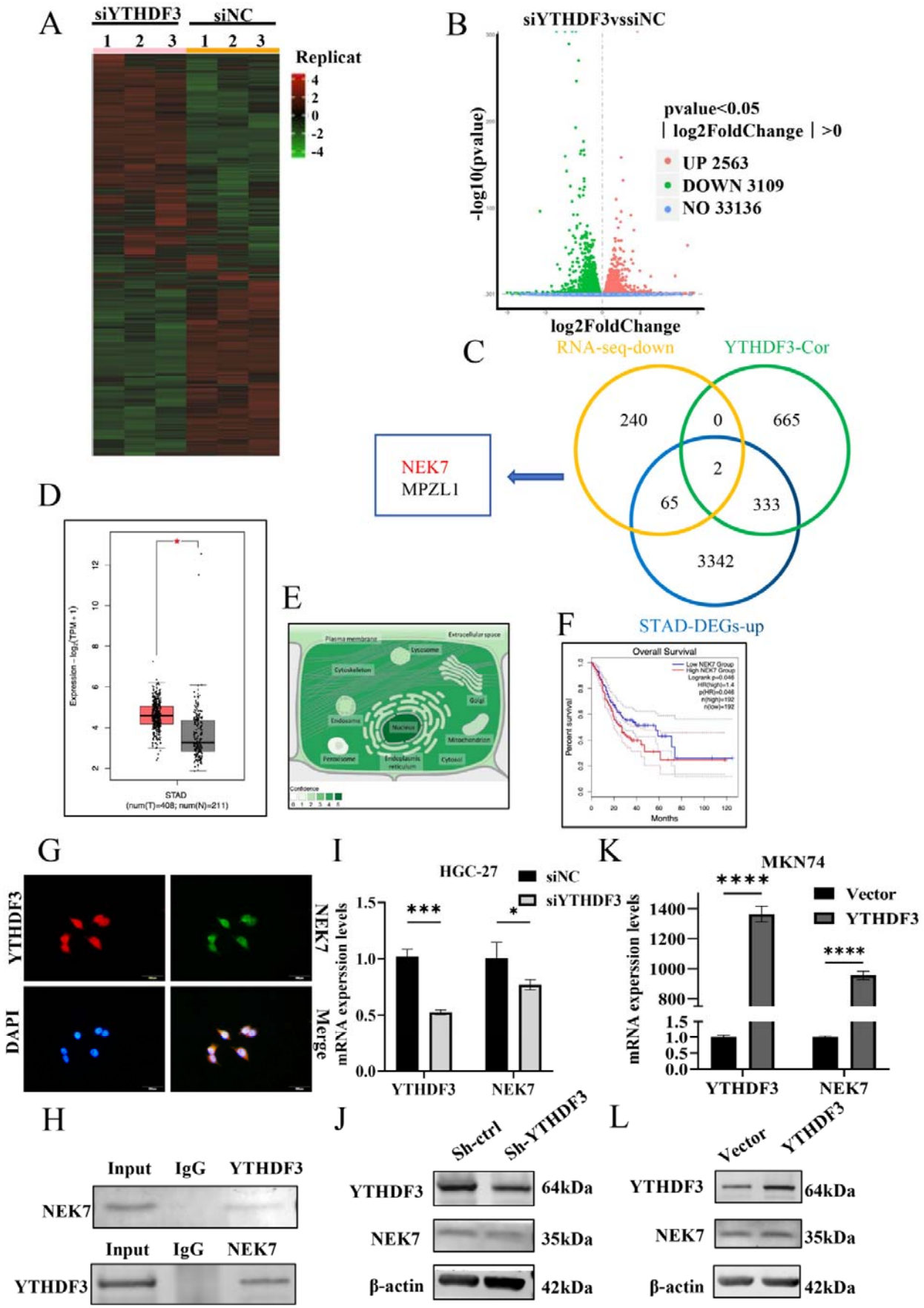
A
siYTHDF3
siNC
1 2 3 1 2 3
Replicat
4
2
0
-2
-4
B
siYTHDF3vssiNC
pvalue<0.05
| log2FoldChange | >0
UP 2563
DOWN 3109
NO 33136
-log10(pvalue)
log2FoldChange
C
RNA-seq-down
YTHDF3-Cor
240
0
665
2
65
333
3342
NEK7
MPZL1
D
Expression - log2(TPM + 1)
STAD
(num(T)=408; num(N)=211)
E
Plasma membrane
Extracellular space
Lysosome
Cytoskeleton
Golgi
Endosome
Nucleus
Mitochondrion
Peroxisome
Endoplasmic reticulum
Cytosol
Confidence
F
STAD-DEGs-up
Overall Survival
Low NEK7 Group
High NEK7 Group
Percent survival
Months
G
YTHDF3
DAPI
Merge
I
HGC-27
siNC
siYTHDF3
NEK7
mRNA experssion levels
***
*
YTHDF3
NEK7
K
MKN74
Vector
YTHDF3
****
****
mRNA experssion levels
YTHDF3
NEK7
H
Input
IgG
YTHDF3
NEK7
Input
IgG
NEK7
YTHDF3
J
Sh-ctrl
Sh-YTHDF3
YTHDF3
64kDa
NEK7
35kDa
β-actin
42kDa
L
Vector
YTHDF3
YTHDF3
64kDa
NEK7
35kDa
β-actin
42kDa

Figure 5. NEK7 is the modification target of YTHDF3. (A) Differential expression genes (DEGs) heat map identified by RNA-seq. (B) The number of DEGs identified by RNA-seq. (C) Overlap analysis of RNA-seq, YTHDF3-cor and STAD-DEGs-up identified genes. (D) Expression of YTHDF3 in GC paired tissue cohort from the TCGA database. (E) Subcellular localization of NEK7 from GeneCards. (F) The survival analysis of NEK7 expression levels and overall survival in patients with GC. (G, H) the interaction between YTHDF3 and NEK7 was verified by Co-IF (G) and Co-IP (H) experiments. Scale bar, 10μm. (I) qRT-PCR was used to detect NEK7 mRNA expression after YTHDF3 knockdown in HGC-27 cells. (J) WB was used to detect NEK7 protein expression after YTHDF3 knockdown in HGC-27 cells. (K) qRT-PCR was used to detect NEK74 mRNA expression after YTHDF3 overexpression in MKN74 cells. (L) WB was used to detect NEK7 protein expression after YTHDF3 overexpression in MKN74 cells. Data are presented as means ± SD. ***P <0.001, ****P <0.0001

Figure 6

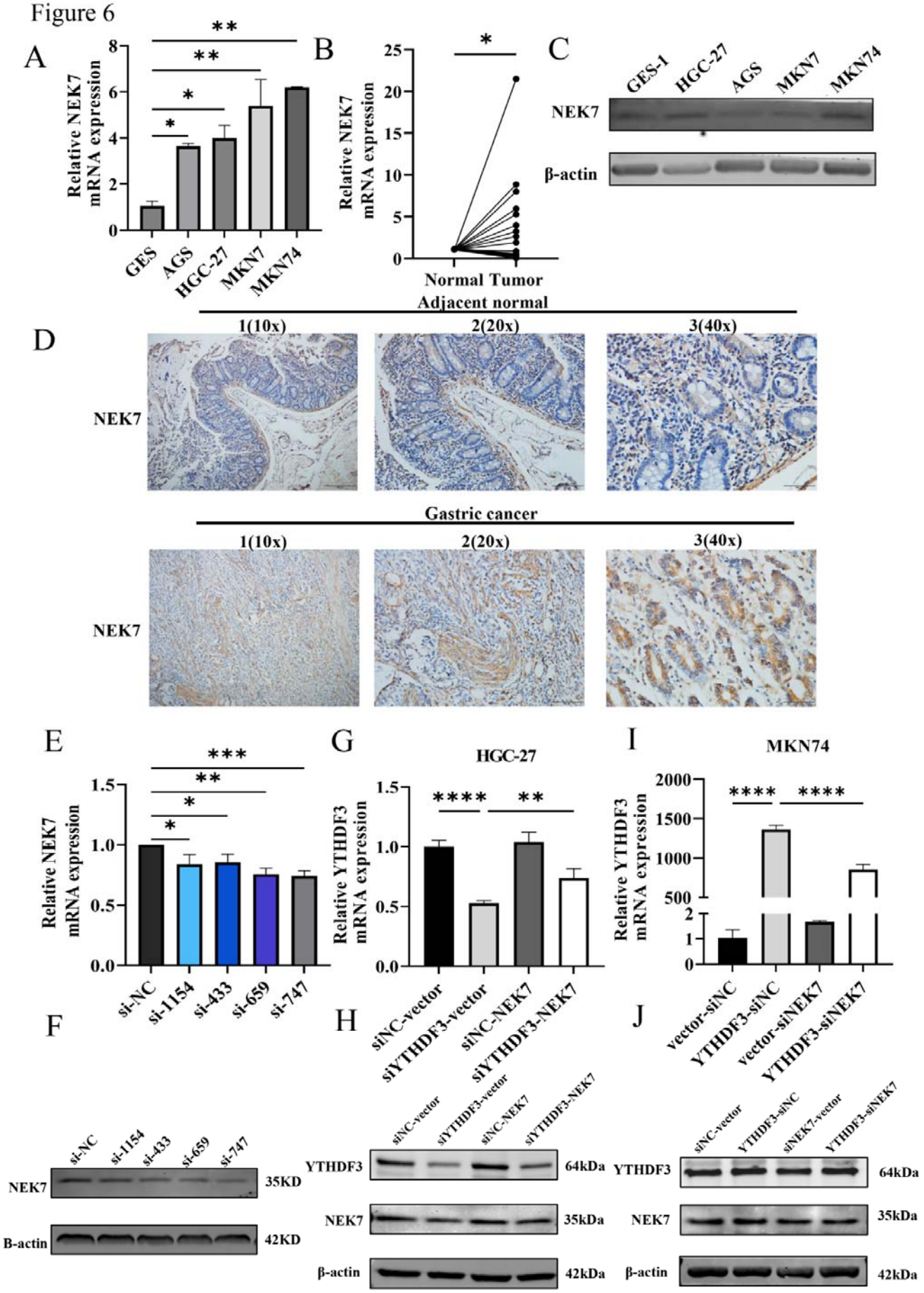
A
Relative NEK7 mRNA expression
GES
AGS
HGC-27
MKN7
MKN74
B
Relative NEK7 mRNA expression
Normal Tumor
Adjacent normal
C
GES-1
HGC-27
AGS
MKN7
MKN74
NEK7
β-actin
D
1(10x)
2(20x)
3(40x)
NEK7
Gastric cancer
E
Relative NEK7 mRNA expression
si-NC
si-1154
si-433
si-659
si-747
G
HGC-27
Relative YTHDF3 mRNA expression
siNC-vector
siYTHDF3-vector
siNC-NEK7
siYTHDF3-NEK7
I
MKN74
Relative YTHDF3 mRNA expression
vector-siNC
YTHDF3-siNC
vector-siNEK7
YTHDF3-siNEK7
F
NEK7
35KD
B-actin
42KD
H
YTHDF3
64kDa
NEK7
35kDa
β-actin
42kDa
J
YTHDF3
64kDa
NEK7
35kDa
β-actin
42kDa

Figure 6. Expression of NEK7 and its interaction with YTHDF3 in GC. (A) The expression ofNEK7 mRNA in GC cell lines and GES-1 was detected by qRT-PCR. **(B)** The expression of NEK7 mRNA in 18 pairs of GC paired tissues was detected by qRT-PCR. **(C)** The basal expression of NEK7 protein in cell lines was detected by WB. **(D)** The expression of YTHDF3 protein in 44 pairs of GC paired tissues was detected by IHC. Scale bar, 50 μm. **(E-F)** Four siRNA-NEK7 sequences were transfected simultaneously into MKN74 cells. **(G-I)** The relative expression level of YTHDF3 mRNA and protein were detected by qRT-PCR and WB after instantaneous co-transfection of YTHDF3 siRNA and NEK7 overexpression plasmid in HGC-27. **(I-J)** The relative expression level of YTHDF3 mRNA and protein were detected by qRT-PCR and WB after instantaneous co-transfection of NEK7 siRNA and YTHDF3 overexpression plasmid in MKN74. Data are presented as means ± SD. ***P <0.001, ****P <0.0001

Figure 7

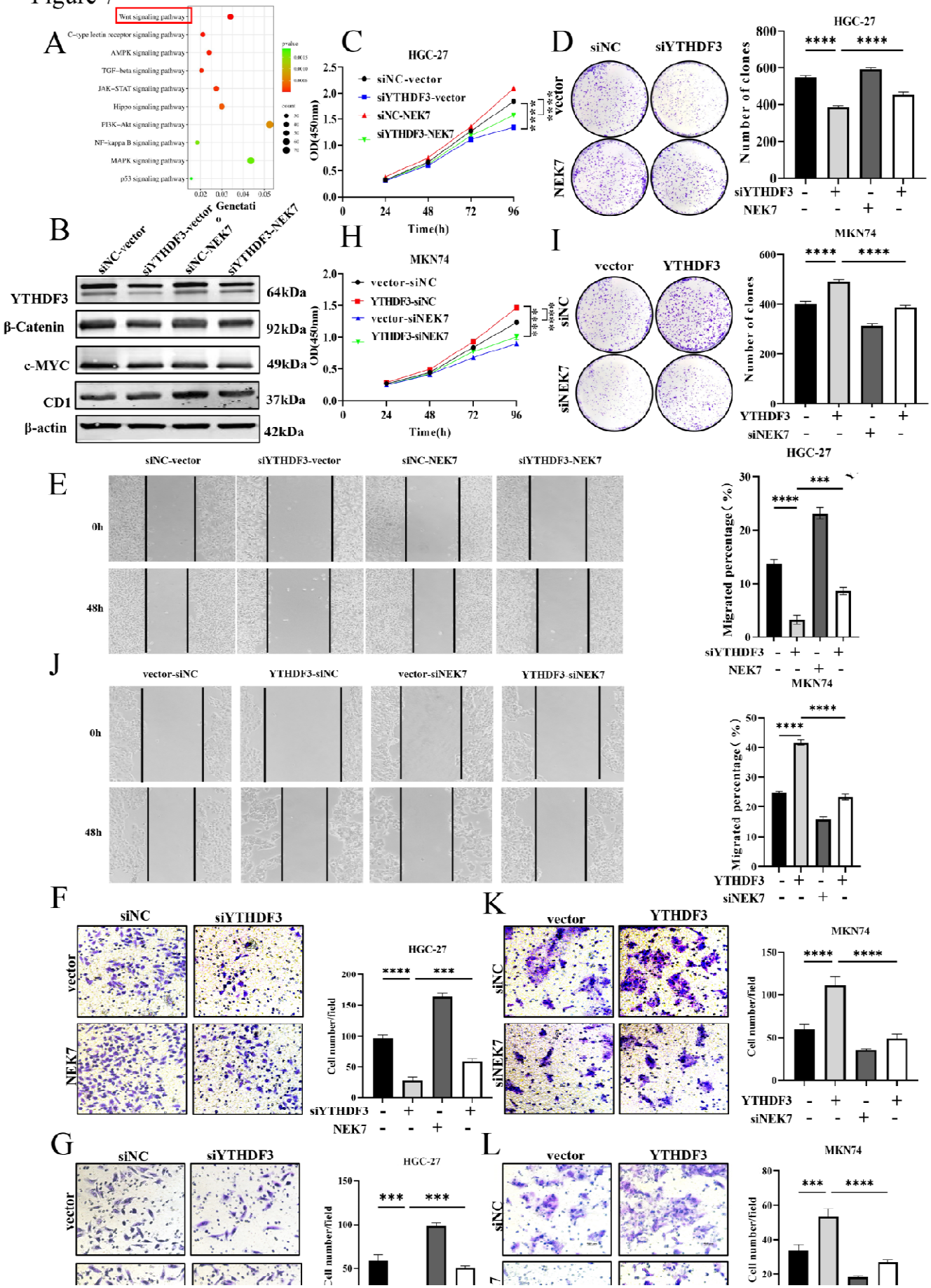
A
Wnt signaling pathway
C-type lectin receptor signaling pathway
AMPK signaling pathway
TGF-beta signaling pathway
JAK-STAT signaling pathway
Hippo signaling pathway
PI3K-Akt signaling pathway
NF-kappa B signaling pathway
MAPK signaling pathway
p53 signaling pathway
Genetio
B
siNC-vector
siYTHDF3-vector
siNC-NEK7
siYTHDF3-NEK7
YTHDF3
β-Catenin
c-MYC
CD1
β-actin
64kDa
92kDa
49kDa
37kDa
42kDa
C
HGC-27
siNC-vector
siYTHDF3-vector
siNC-NEK7
siYTHDF3-NEK7
OD(450nm)
Time(h)
D
siNC
siYTHDF3
vector
NEK7
HGC-27
Number of clones
siYTHDF3
NEK7
H
MKN74
vector-siNC
YTHDF3-siNC
vector-siNEK7
YTHDF3-siNEK7
I
vector
YTHDF3
siNC
siNEK7
MKN74
E
siNC-vector
siYTHDF3-vector
siNC-NEK7
siYTHDF3-NEK7
0h
48h
Migrated percentage (%)
J
vector-siNC
YTHDF3-siNC
vector-siNEK7
YTHDF3-siNEK7
F
Cell number/field
K
L

Figure 7. Oncogenic function of YTHDF3 depends on NEK7 and Wnt/β-catenin signaling pathway.

(7A) KEGG enrichment result of the differentially expressed gene sets from the RNA-seq. (7B) The expression levels of Wnt/β-catenin signaling pathway related proteins were detected by WB after instantaneous co-transfection of YTHDF3 siRNA and NEK7 overexpression plasmid in HGC-27. (C, E, G, I, K) The effects of NEK7 on YTHDF3 in HGC-27 cells were detected by CCK-8 assay (C), colony formation assay (E), wound healing assay (G),Scale bar, 200 μm, Transwell migration assay (I) and Transwell invasion assay (K). Scale bar, 100 μm. (D, F, H, J, L) The effects of NEK7 on YTHDF3 in MKN74 cells were detected by CCK-8 assay (D), colony formation assay (F), wound healing assay H), Scale bar, 200 μm, Transwell migration assay (J) and Transwell invasion assay (L). Scale bar, 100 μm.. Data are presented as means ± SD. $^{*}P < 0.05$, $^{**}P < 0.01$, $^{***}P < 0.001$, $^{****}P < 0.0001$